Strong aerosol indirect radiative effect from dynamic-driven diurnal variations of cloud water adjustments

Jiayi Li[1]†, Yang Wang[1]†, Jiming Li[1*], Weiyuan Zhang[1], Lijie Zhang[1], Yuan Wang[1]

[1] Collaborative Innovation Center for Western Ecological Safety, College of Atmospheric Sciences, Lanzhou University, Lanzhou 730000, China.

Correspondence to: Jiming Li (lijiming@lzu.edu.cn)

† These authors contributed equally to this work.

Abstract. Aerosol-cloud interaction (ACI) is the critical yet most uncertain process in future climate projections. A major challenge is the sign and magnitude of cloud liquid water path (LWP) response to aerosol perturbations (represented by cloud droplet number concentration, N_d) at different temporal and spatial scales are highly variable, but potential microphysical-dynamical mechanisms are still unclear, especially at a diurnal scale. Here, robust observational evidence from geostationary satellite reveals that the diurnal variation of LWP adjustments is driven primarily by diurnal-related boundary layer decoupling and cloud-top entrainment. Strikingly, these diurnal adjustments exhibit a distinct regional pattern associated with cloud regimes. We find that the cooling effect of LWP adjustments would be underestimated by up to 89% in study regions if neglecting their diurnal variations, leading to a further 20% offset of Twomey effect, thus biasing aerosol indirect effect toward a warming direction. Our findings highlight the key role of diurnal variation of ACI in reducing the uncertainty in climate projections.

1 Introduction

Marine low-level clouds (MLCs), which cover one-third of the global ocean (Klein and Hartmann, 1993), exert a strong cooling effect by reflecting the incoming solar radiation back into space (Jiang et al., 2023). Their reflectivity to solar radiation is highly sensitive to atmospheric aerosol concentrations because aerosols can serve as the cloud condensation nuclei (CCN) to modify the mediated variables (e.g. droplet number concentrations, N_d; effective radius, r_e) of aerosol-cloud interactions (ACI). ACI contributes the largest uncertainty of aerosol radiative forcing and future climate projections. Aerosol-induced increases in CCN can enhance N_d and hence reduce r_e, boosting cloud albedo while holding cloud liquid water content (the Twomey effect) (Twomey, 1977). Additional alterations in cloud microphysics may arise from changes in the quantity of liquid water or cloud cover that are induced by aerosol variations. These changes can lead to rapid adjustments within the cloud in response to aerosol perturbations, indicating that the impact of aerosols on cloud properties is multifaceted (Bellouin et al., 2020). For example, it has been documented that liquid water path (LWP) can either increase due to precipitation suppression (positive LWP adjustments) (Albrecht, 1989) or decrease due to entrainment feedbacks (negative LWP

adjustments) (Ackerman et al., 2004; Bretherton et al., 2007; Small et al., 2009). While the Twomey effect is well-recognized, however, LWP adjustments are highly uncertain as the least understood and most poorly quantified in all climate forcing (IPCC, 2023).

These large uncertainties in LWP adjustments are generally attributed to the complex interplay of microphysical-dynamical conditions and aerosol loading (represented by N_d) that vary with different temporal and spatial scales (Bender et al., 2019; Chen et al., 2014; Glassmeier et al., 2021; Gryspeerdt et al., 2022a). Numerous observational studies have been carried out to understand the extent of this variability and uncertainties of LWP adjustments, with the aim of constraining model simulations (Gryspeerdt et al., 2019, 2021; Rosenfeld et al., 2019; Trofimov et al., 2020; Wilcox, 2010). These investigations have spanned various regions and targets, revealing diverse cloud responses attributable to the varied mechanisms of LWP adjustments. In addition, it has been confirmed that analysis methods, sampling strategies, and meteorology covariations could be a considerable other source of uncertainty in LWP adjustments (Chen et al., 2014; Gryspeerdt et al., 2022b; Rosenfeld et al., 2019, 2023). Here, we focus on the time-dependence of LWP adjustments (i.e., diurnal variations) as it is associated with both sampling strategies and meteorology covariations. It has been established that marine cloud properties and the cloud-topped marine boundary layer exhibit prominent diurnal variations in response to solar radiation, which are closely related to their regional dependence (Duynkerke and Hignett, 1993; Wood et al., 2002). The microphysical-dynamical boundary layer feedback, which generally covaries with regional diurnal cycle, could augment or weaken the LWP adjustments and thus lead to the diurnal variation of LWP adjustments with broad spreads and even different signs. This means that a one-size-fits-all approach to global-mean LWP adjustments may not provide a robust constraint, given the regional and temporal mechanisms at play (Michibata et al., 2016). Additionally, the microphysical-dynamical mechanisms behind are complex and still poorly understood (Feingold et al., 2024). This drives the speculation that the diurnal variations of LWP adjustments could be one of the most significant yet overlooked sources of uncertainty of ACI.

However, to date, a majority of studies have relied on observations from polar-orbiting satellites to investigate the spatial distribution and long-term variations of N_d (Bennartz and Rausch, 2017; Li et al., 2018; McCoy et al., 2018), which are insufficient to depict the time-dependent nature of LWP adjustments. Based on Himawari-8 geostationary satellite, the diurnal variations of cloud microphysical properties and LWP adjustments in two typical regions as selected, and the associated influencing factors and mechanisms are presented in this study. Our research aims to expand our understanding of the influence of meteorological factors, initial aerosol states (specially N_d), and the covariance between meteorology and aerosols on cloud LWP, gaining a comprehensive understanding of the diurnal variations in LWP adjustments which is a highly time-dependent variable lacking quantification, in conjunction with shifts in regional meteorological conditions.

2 Data and Methods

Our analysis focuses on 1° × 1° non-precipitation marine low-level cloud samples, aggregated from filtered pixel-level satellite data. We aim to avoid the impact of precipitation on retrieval of N_d and focus only on the development of clouds in

response to aerosol loading associated with microphysical-dynamical conditions over two selected regions. One is located in the west of Australia (25º-35ºS, 95º-105ºE, AUW). The other is in the East China Sea (20º-30ºN, 120º-130ºE, ECS), as shown in Figure S1 in Supplementary Materials.

2.1 N_d retrieval based on geostationary satellite product

In this study, 4 years (2016-2019) of hourly cloud microphysical properties data from the Satellite Cloud and Radiation Property retrieval System (SatCORPS) Clouds and the Earth's Radiant Energy System (CERES) Geostationary Satellite (GEO) Edition 4 Himawari-8 over the Northern Hemisphere (NH) (Southern Hemisphere (SH)) Version 1.2 data product (CER_GEO_ED4_HIM08_NH_V01.2, CER_GEO_ED4_HIM08_SH_V01.2) were collected (NASA/LARC/SD/ASDC, 2018b, a). The datasets are derived from the Advanced Himawari Imagers (AHI) on Himawari-8 geostationary satellite, using the Langley Research Center (LARC)s SatCORPS algorithms in support of CERES project (Minnis et al., 2021; Trepte et al., 2019). The retrievals are at 2-km resolution (at nadir) and are sub-sampled to 6 km. The sub-sampled resolution meets the needs of the CERES project without having a data implosion. The cloud optical thickness (CLOT), cloud effective radius (r_e) and cloud-top temperature (CLTT) from the SatCORPS product during the daytime were used to retrieve N_d in our study. Other cloud properties such as cloud-top height (CLTH), cloud base height (CLBH) and cloud thickness (H) were used in further analysis. The SatCORPS is based on the CERES Ed4 cloud retrieval algorithm, providing more accurate CLTH and H parameterizations (Minnis et al., 2011, 2021). Briefly, CLTH is estimated as the altitude where the cloud-top temperature (CLTT) occurs in the temperature profile. The temperature profile is provided by CERES Meteorology, Ozone, and Aerosol (CERES MOA) dataset. CLTT is derived from an empirical parameterization of cloud-top emissivity at channel 4 and cloud effective temperature. H is computed using empirical formulas with τ: $\mathrm{H} = 0.39 \ln \tau - 0.01$ for liquid clouds. CLBH is directly obtained by subtracting H from CLTH.

The SatCORPS retrievals provide cloud effective radius (r_e) in the 3.9 μm near-infrared band (Kang et al., 2021), which is closest to the cloud top with less bias in further calculation of N_d (Grosvenor et al., 2018). N_d can be estimated as (Bennartz, 2007):

$$N_d = \frac{\sqrt{5}}{2\pi k}\left(\frac{f_{ad} c_\omega \tau}{Q \rho_w {r_e}^5}\right)^{\frac{1}{2}} \quad (1)$$

where τ represents cloud optical depth and ρ_w is liquid water density. The extinction efficiency $Q \approx 2$, as Q relies less on the size parameter in near-infrared. k, related to droplet size distribution, is set as 0.8 for maritime cloud (Martin et al., 1994; Painemal and Zuidema, 2011). c_w represents the condensation rate determined by temperature in cloud (here is the cloud-top temperature from SatCORPS). A constant adiabatic value (f_{ad}) of 0.8 is used to represent the deviation from the adiabatic profile (Bennartz, 2007). This is the most common method to derive N_d from passive satellite observations (Bennartz, 2007; Bennartz and Rausch, 2017; Li et al., 2018; McCoy et al., 2018) and has been validated as a reliable technique for observing changes in long-term variations of N_d (Boers et al., 2006). Li et al. (2018) demonstrated that passive satellite N_d retrievals exhibit strong consistency with active satellite retrievals. The SatCORPS Himawari-8 retrievals agree well with in-situ

observations according to Kang et al. (2021). In this study, the LWP from SatCORPS is calculated as $\frac{5}{9}\rho_w \tau r_e$ in sub-adiabatic conditions, following the method by Wood and Hartmann (2006). The combination of these two retrieval methods of N_d and LWP has been widely used in the satellite investigations of LWP adjustment (Fons et al., 2023; Gryspeerdt et al., 2019; Qiu et al., 2023; Smalley et al., 2024).

Several sampling strategies were adopted in this study to select cloud pixels to meet the above retrieval assumptions (Grosvenor et al., 2018; Gryspeerdt et al., 2019; Li et al., 2018). Only pixels in the liquid phase with cloud-top temperature warmer than 268 K under 3.2 km were included. To maintain consistency with previous studies (Bennartz and Rausch, 2017; Li et al., 2018), we adopted 268 K as the threshold of CLTT for liquid clouds, rather than 273 K. In fact, 96% (97%) of the samples exhibited CLTT above 273 K in AUW (ECS) region. Therefore, the threshold has a negligible impact on the overall results. The lower bounds of r_e (τ) were set as 4 μm (4) to reduce uncertainties. Moreover, pixels with solar zenith angles larger than 65° were excluded. Filtered data was used to calculate N_d and then aggregated to 1° × 1° grid. Each grid containing at least 30 pixels is considered a cloud sample. On average, each grid contains 83 (87) pixels in AUW (ECS) region.

We followed the previous methods to filter cloud pixels. But this classification only limits cloud top properties and cloud phase, inevitably including different cloud regimes, such as low-level cumulus clouds. This might introduce uncertainties as cumulus clouds and stratocumulus clouds have different adiabatic properties but we have set the adiabatic rate as a constant value in the retrieval process. Uncertainties may occur as f_{ad} varies with cloud depth (Grosvenor et al., 2018; Min et al., 2012). As acquiring hourly f_{ad} on a global scale is difficult, to date, studies investigating diurnal variations based on geostationary satellites continue to employ a constant f_{ad} value (Fons et al., 2023; Qiu et al., 2024; Smalley et al., 2024). Also, the choices of constant k might introduce bias into the retrieval of N_d. Studies have found that k parameter varied with the height within cloud and cloud types (Brenguier et al., 2011; Martin et al., 1994; Painemal and Zuidema, 2011). Since the bias caused by the retrieval contributes equally to all samples, it may change the magnitude of variables without changing the diurnal patterns or the mechanisms behind them. Consequently, the above uncertainties will not greatly affect the conclusions of this paper.

To minimize the influence of precipitation, particularly the bias introduced in N_d and LWP retrievals due to invalidating the adiabatic (or sub-adiabatic) assumption, only non-precipitating clouds are discussed in this study. Therefore, GPM IMERG Final Precipitation L3 Half Hourly 0.1 degree x 0.1 degree V07 (GPM_3IMERGHH) was used as a precipitation criterion (Huffman et al., 2020). To align these two satellite products, SatCORPS cloud pixels within each 0.1° grid of GPM_3IMERGHH are assigned the same precipitation value. Cloud samples are regarded as non-precipitation only if the GPM_3IMERGHH precipitation rate equals 0 mm/hr in 1° × 1° grid. In total, we collect 480189 cloud samples in AUW and 173181 cloud samples in ECS using 4-year (2016-2019) hourly record from SatCORPS Himawari-8.

2.2 Quantification of LWP adjustments

To quantify LWP response, both direct and indirect methods have been used in previous studies. The logarithmic relationship between N_d and LWP ($\frac{\partial \ln LWP}{\partial \ln N_d}$) is a direct way to quantify LWP sensitivity to aerosol perturbations, where N_d is

considered a proxy of CCN. Another indirect way of describing the variation of cloud water due to aerosols ($-\frac{\Delta \ln \tau}{\Delta \ln r_e}$) is deduced from the contributions of changes in LWP and r_e to the changes in cloud optical depth ($\frac{\Delta \tau}{\tau} = \frac{\Delta \mathrm{LWP}}{\mathrm{LWP}} - \frac{\Delta \mathrm{r_e}}{\mathrm{r_e}}$) (Christensen and Stephens, 2011; Coakley and Walsh, 2002). Whereas the latter method is put forward with a default condition that Δr_e is always negative, it is only applicable to small-scale pollution tracks like industry tracks, volcano tracks or ship tracks, etc. (Rahu et al., 2022; Toll et al., 2019). Therefore, the former method is applied in this study, which has been commonly used in researches on aerosol-cloud interactions based on large-scale satellite observations (e.g., Glassmeier et al., 2021; Gryspeerdt et al., 2019; Rosenfeld et al., 2019).

LWP adjustment at any given moment is the result of all available data at that moment. The regression slope of N_d and LWP in log-log space ($\frac{\partial \ln LWP}{\partial \ln N_d}$) is calculated on 1° grid scale. Following previous studies (Fons et al., 2023; Rosenfeld et al., 2019), we choose the median LWP in each ln(N_d) bin as the feature point for the entire sample space making the regression more representative of the overall characteristics of all samples (black dots in Figure 1, A and D). Since the relationship between N_d and LWP in non-precipitation clouds shows a non-linear trend in ECS region, turning points in N_d with the lowest LWP are found to characterize LWP adjustments with two different N_d stages (i.e., purple and blue lines in Figure 1D).

2.3 Reanalysis datasets

Aerosol property is represented by the total column extinction optical depth (AOD) at 550 nm from hourly time-averaged 2-dimensional data collection in Modern-Era Retrospective analysis for Research and Applications version 2 (MERRA-2), with a spatial resolution of 0.5° × 0.625° (Buchard et al., 2017). It is interpolated onto a 1° × 1° grid using bilinear interpolation method.

Meteorological indicators related to cloud microphysical process are either obtained or calculated by ERA5 reanalysis data (Hersbach et al., 2020), including sea surface temperature (SST), lower-tropospheric stability (LTS), relative humidity on 700 hPa and 1000 hPa (RH700 and RH1000), vertical velocity on 700 hPa (omega700) and 800 hPa (omega800), horizontal wind field on 700 hPa and horizontal temperature advection at the surface ($\mathrm{SST_{adv}}$). The ERA5 is the fifth-generation atmospheric reanalysis of global climate and is produced using the ECMWF's Integrated Forecast System cycle 41r2 with a 4-dimension variation assimilation system. Compared to the ERA-Interim, the ERA5 has higher spatial (0.25° × 0.25°) and temporal resolutions (hourly), and the representation of atmospheric processes has been further improved. In this study, the ERA5 reanalysis data is matched to SatCORPS data in the same way as GPM_3IMERGHH.

The LTS is expressed as the difference of potential temperature between 700 hPa and the surface (Klein and Hartmann, 1993). For the horizontal temperature advection at the surface ($\mathrm{SST_{adv}}$), it is expressed in spherical coordinate as Jian et al. (2021) and Qu et al. (2015):

$$\mathrm{SST}_{adv} = -\frac{\mathrm{u}}{\mathrm{R_E}\cos\phi}\frac{\partial \mathrm{SST}}{\partial \lambda} + \frac{\mathrm{v}}{\mathrm{R_E}}\frac{\partial \mathrm{SST}}{\partial \phi} \quad (2)$$

where $\mathrm{R_E}$ is the mean Earth radius, SST is the surface skin temperature, u and v are the eastward and northward horizontal 10

m wind components, respectively. Φ and λ represent the radians of latitude and longitude. A positive/negative SST_{adv} indicates warm/cold advection, which influences the surface latent and sensible heat fluxes then the moisture transport within the cloud layer and the cloud thickness (George and Wood, 2010) and, consequently, influences the cloud liquid water.

3 Results

3.1 LWP adjustments vary alongside microphysical-dynamical conditions

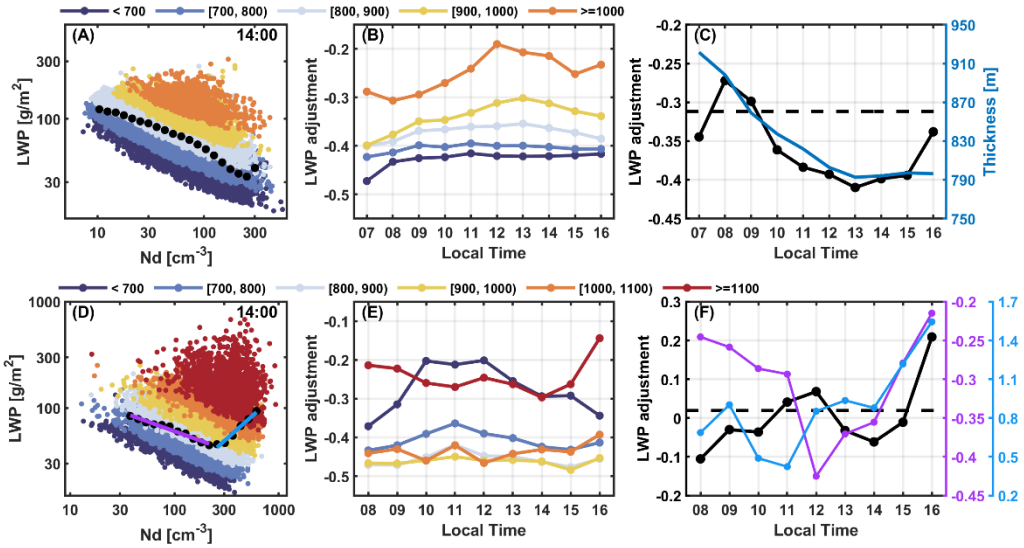

Figure 1. LWP adjustments in log-log spaces and their diurnal patterns in two typical regions (the west of Australia, AUW and the east China sea, ECS). Non-precipitation cloud samples are scattered in N_d-LWP log space at 1400 LT in (A) AUW and (D) ECS region. Colored dots are samples in different cloud thickness (H) bins (unit: m). Black dots represent the median LWP in each N_d bin. The colored lines are the fits of black dots at different stages in ECS region. Diurnal variations of LWP adjustments binned by H in (B) AUW and (E) ECS regions are shown. Colored lines in (F) are diurnal variations of different stages in (D), while black lines in (C) and (F) are the overall diurnal variations of LWP adjustments in two regions, respectively. The blue line in (C) represents the diurnal variation of H. Dashed lines represent the average LWP adjustments considering diurnal variations, –0.31 for AUW (C) and 0.02 for ECS (F).

Figure 1 (A and D) shows the scatter plots of N_d-LWP relationship in log-log space for AUW and ECS regions at 1400 LT (local time), respectively. The complete pictures of all available daytime periods are presented in Figure S2. The N_d-LWP relationships show similar patterns during daytime in each region but different results in two regions, with an overall negative adjustment in AUW, meaning that LWP decreases with increased N_d, while the LWP adjustments in ECS region exhibit both positive and negative throughout the day. For non-precipitation clouds, both positive and negative LWP adjustments have been

reported (Glassmeier et al., 2021; Michibata et al., 2016; Rosenfeld et al., 2019; Toll et al., 2019) and attributed to different mechanisms (e.g., lifetime effect and entrainment feedbacks) (Michibata et al., 2016). In fact, the sign of LWP adjustment is ultimately subject to the dominant microphysical-dynamical mechanisms for each N_d stage. Before about 300 cm^{-3}, LWP adjustments are dominated by processes at the cloud margins, such as sedimentation-entrainment feedback (Ackerman et al., 2004) and evaporation-entrainment feedback (Small et al., 2009), leading to negative LWP adjustments in both regions (Figure 1A and purple line in Figure 1D).

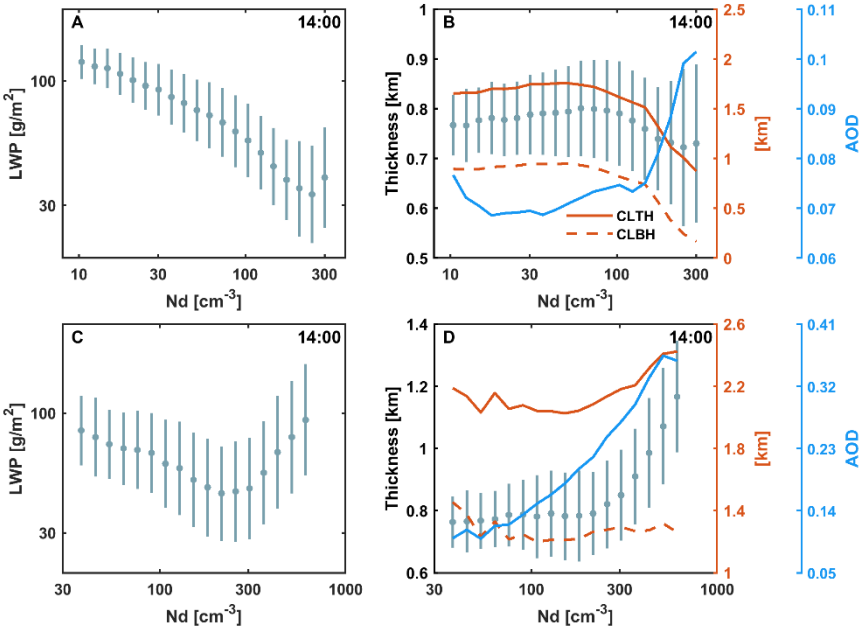

Figure 2. Comparisons between N_d-LWP relationship and N_d-Thickness relationship in two regions. Relationship between N_d and (A) LWP, (B) cloud thickness in AUW region. Relationship between N_d and (C) LWP, (D) cloud thickness in ECS region. The orange solid and dashed lines show the change of cloud top height (CLTH) and cloud base height (CLBH) with N_d.

However, LWP begins to rise at high N_d in ECS (blue line in Figure 1D), which is the primary reason causing the overall positive LWP adjustments in this region. Positive sensitivity over ECS has been reported but not fully understood (Bender et al., 2019; Gryspeerdt et al., 2019; Zhang et al., 2021). Michibata et al. (2016) attributed the positive LWP response in non-precipitation clouds over East Asia to the cloud lifetime effect (Albrecht, 1989). Here in ECS region, clouds are heavily affected by anthropogenic aerosols, showing LWP increases with N_d at high N_d (>300 cm^{-3}). This behavior is related to the deepening of cloud depth with aerosols (Figure 2, C and D), indicating warm invigoration by aerosols (Koren et al., 2014).

The above opposite responses of LWP (either enhanced or decreased) to increasing aerosol loading depends on the environmental conditions and cloud characteristics (Altaratz et al., 2014). On the one hand, they indicated that more droplets

delay the collision-coalescence and provide more surface area for condensation, releasing latent heat and promoting cloud vertical development, thus increasing LWP (warm invigoration). On the other hand, more small droplets can be more likely to evaporate due to enhanced entrainment, leading to a decreased LWP (entrainment feedbacks). According to Dagan et al. (2015), the competition between these two processes determines the response of cloud macrophysical properties to aerosols. The N_d-LWP relationship in ECS indicates that warm invigoration takes over after around 300 cm^{-3} leading to cloud deepening. Here, we will demonstrate that ECS region is favorable for warm invigoration to occur from three aspects: environmental conditions, cloud regimes and aerosols.

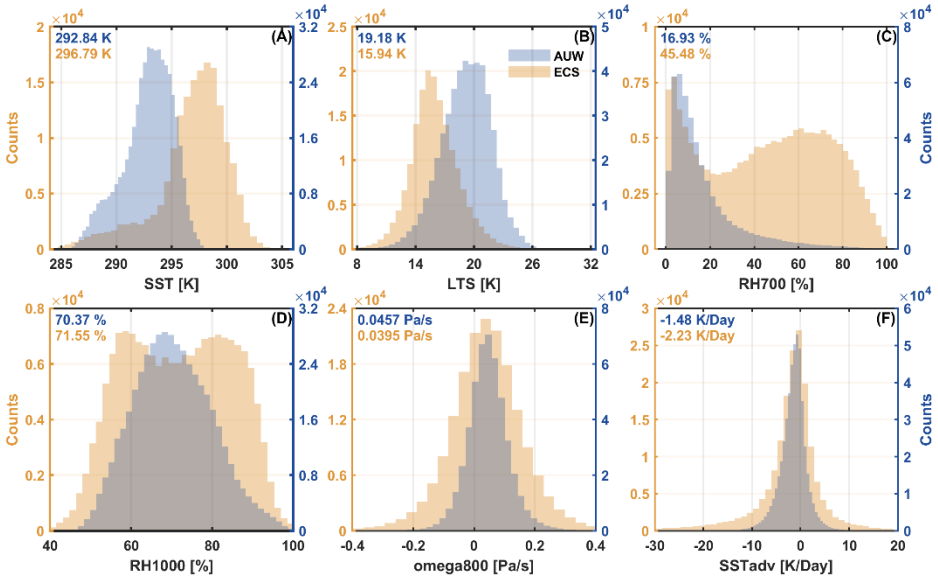

Figure 3. 4-year meteorological conditions of non-precipitation clouds in AUW and ECS regions from 2016 to 2019. Histograms of meteorological factors are presented here. The mean values are labeled in the top-left corner. Data are directly or indirectly derived from ERA5. For vertical velocities on 800 hPa (omega800), positive (negative) values indicate downdraft (updraft).

Although the microphysical-dynamical processes are challenging to observe directly, environmental conditions can be considered as proxies and provide further support for the invigoration effect. The cloud deepening in ECS region is mainly attributed to increasing CLTH (Figure 2D). Unstable boundary layers (low LTS) favor the formation of more convective clouds (Manshausen et al., 2022), while high RH provides moisture for cloud vertical development. The unstable and moist atmosphere in ECS provides such conditions with a mean lower-tropospheric stability (LTS) of 15.94 K and a peak in relative humidity on 700 hPa (RH700) of 70% (Figure 3). Gryspeerdt et al. (2019) also reported this rising behavior at high N_d, especially in moist conditions, consistent with our results noted here. Christensen and Stephens (2011) found elevated cloud-top height from open cell clouds in response to ship pollution in relatively unstable and moist conditions.

Secondly, the more prevalent convective clouds in the ECS region would be another favorable condition for warm

invigoration. Zhang et al. (2021) also attributed the positive LWP adjustments to warm invigoration with the widespread low-level convective clouds (Sc and Cu) in ECS. According to the division from Rosenfeld et al. (2019), we categorize the clouds into three regimes, i.e., Sc (LTS > 18 K), Sc to Cu transition (14 K ≤ LTS ≤ 18 K), and Cu (LTS < 14 K). (Figure 4, G, H and I). We show that clouds in ECS region are dominated by the Sc to Cu transition regime. The formation of this transition regime is associated with increasing sea surface temperature (SST) due to "deepening-warming decoupling" (Albrecht et al., 1995; Bretherton and Wyant, 1997). Sc presents over the relatively shallow and stable boundary layer with cooler sea surface along the coast (Figure 4, A and B) and most of Sc may be advected from the southeast Chinese plain (Klein and Hartmann, 1993). According to the cloud advection scheme by Miller et al. (2018), cloud advection can be approximated as a translation of the cloud field with the wind field. The advection height is assumed to correspond to the height of the cloud top. Therefore, we can simply deduce from the wind field on 700 hPa (Figure 4A) that clouds in ECS have the possibility of advection from the Chinese plain in the west. As air moves offshore, MBL deepens and cloud layer decouples with the surface mixed layer over the warmer sea surface. Cu forms in the moist and unstable subcloud layer and rises to the upper cloud layer, resulting in a local cumulus-coupled MBL.

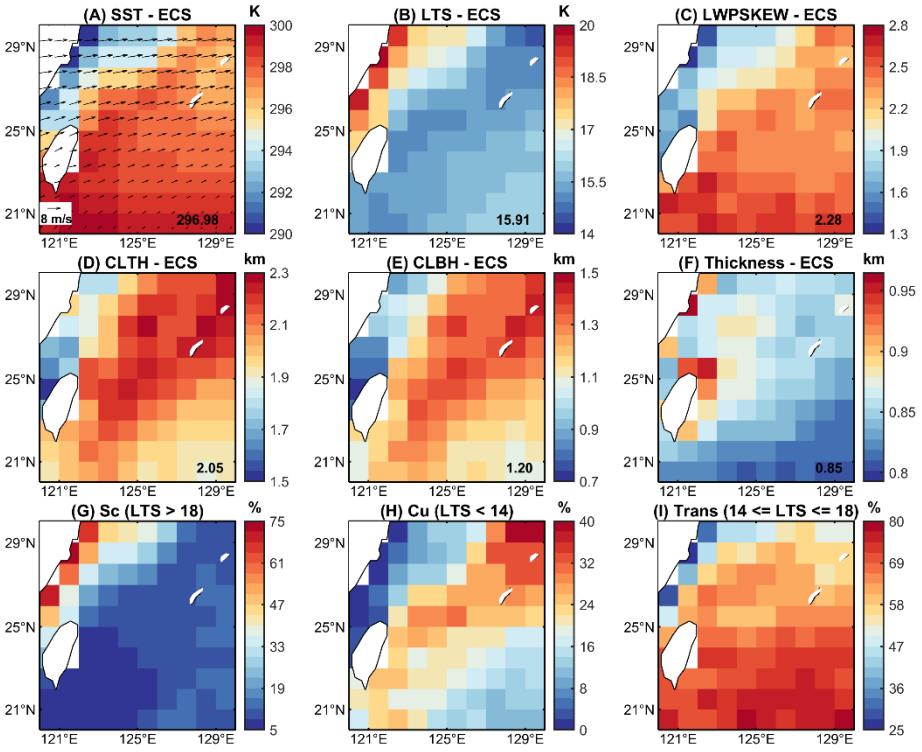

Figure 4. Distributions of meteorological factors and different cloud regimes in ECS region. (A) Sea Surface Temperature (SST), the composite wind field (arrows) on 700 hPa and (B) lower-tropospheric stability (LTS) are from ERA5 reanalysis data. (C) LWP skewness, (D) cloud-top height (CLTH), (E) cloud base height (CLBH) and (F) cloud thickness are directly or

indirectly derived from SatCORPS Himawari-8 product. The numbers in the lower right corner represent regional averages being weighted by the cosine of latitude. Distribution of the proportion of cloud regimes for (G) Stratocumulus (Sc, LTS > 18 K), (H) Cumulus (Cu, LTS < 14 K), (I) Sc to Cu transition regime (Trans, 14 K <= LTS <= 18 K).

Finally, at high aerosol-loading conditions, warm invigoration has been found in numerous studies. For instance, Kaufman et al. (2005) reported larger LWP in higher aerosol loading conditions over Atlantic warm clouds (a mix of stratus and trade cumulus) using MODIS observations. Yuan et al. (2011) found increased cloud amount and higher cloud top heights associated with volcanic aerosols in trade cumulus near Hawaii with A-Train satellites. In contrast to the model results of Koren et al. (2014), who suggested that warm invigoration saturates at higher aerosol loading (AOD ~ 0.3), our findings indicate a higher AOD of 0.41 (Figure 2), which is reasonable because the saturation value of AOD exhibits regional variability. For example, Kaufman et al. (2005) reported a maximum AOD of 0.46, while Zhang et al. (2021) found that the AOD in the ECS region is approximately 0.4. To summarize, these evidences all confirm the plausibility of warm invigoration in the ECS region, causing the positive LWP adjustments at high N_d.

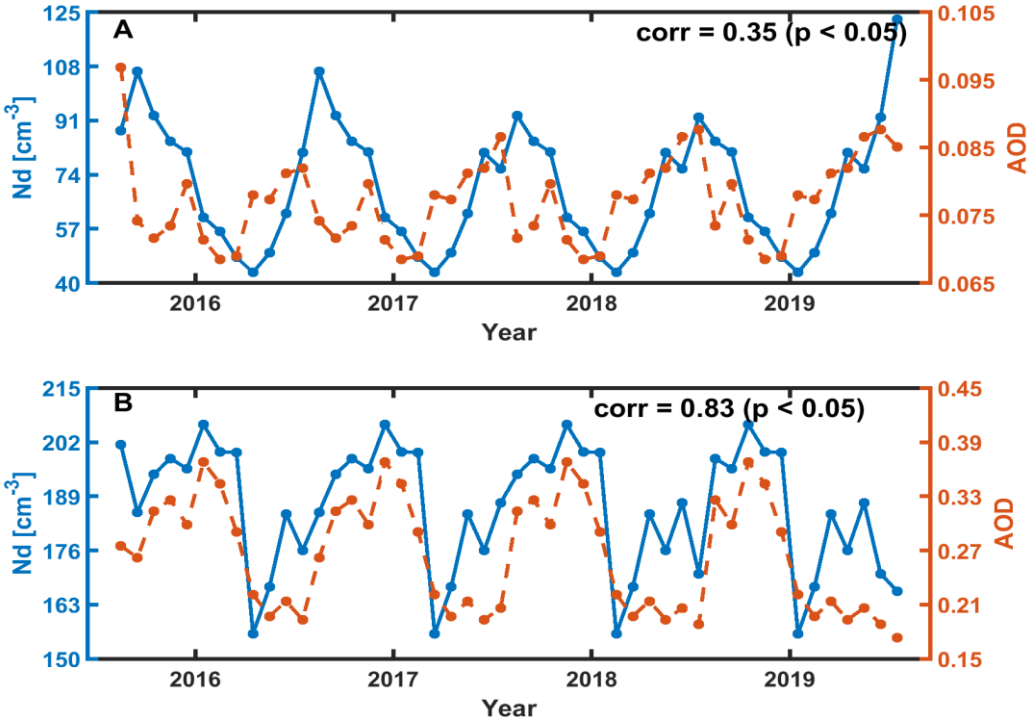

Figure 5. 4-year long-term variations of N_d and total aerosol optical depth (AOD) from MERRA-2 at 1200 LT in AUW (A) and ECS (B) region. The correlation coefficients (corr) between N_d and AOD are 0.35 and 0.83 (significant at the 95% confidence level), respectively.

Note that we select the column AOD as an aerosol proxy to remain consistent with the above studies. Although AOD may not represent aerosol concentrations in some conditions, Figure 5 shows significant correlations observed between the 4-year long-term variations of AOD and N_d at 1200 LT in both regions, particularly in ECS with a correlation of 0.81. Meanwhile, both regions show the similar distribution patterns, with higher N_d and smaller r_e near the continental coastal area, aligning with the average AOD spatial distribution (spatial correlation coefficients of 0.84 in AUW and 0.91 in ECS) (Figure S1), suggesting the availability of AOD as an aerosol proxy.

Furthermore, a sensitivity analysis is conducted to exclude the influence of Simpson's Paradox. Due to thicker cloud samples along the coast with larger N_d and thinner ones with smaller N_d offshore in ECS region, we divide the samples into coastal and offshore groups and find that the observed pattern is not significantly affected by the geographical region (Figure S3). Considering the different processes associated with cloud regimes, we conducted a similar analysis for each cloud regime. Our findings reveal that the pattern of LWP adjustments is insensitive to cloud regime (Figures S4-S6), suggesting that they can be studied collectively.

We further analyze the influence of meteorological conditions (i.e., LTS and RH) on LWP adjustments in the two regions (Figure S7). Overall, LWP adjustments cannot be explained by a single meteorological factor. For example, in ECS region, despite the similarity in diurnal patterns of LWP adjustment within different LTS bins, the magnitudes exhibit significant differences due to different aerosol loadings. Samples with LTS > 18 K are concentrated in coastal areas with higher aerosol loadings. Warm invigoration is stronger for these samples, thus the overall LWP adjustment is positive. In contrast, samples with LTS < 18 K have a larger proportion of smaller aerosol loadings. The effect of entrainment feedback is more pronounced. This further highlights the importance of aerosol loadings in regulating LWP adjustments in ECS region. Meanwhile, the intricate interplay among meteorological factors, clouds, and aerosols makes it difficult to exclude the influences from meteorological factors (Chen et al., 2014; Engström and Ekman, 2010; Zhang and Feingold, 2023).

Previous studies employed various methods to exclude environmental confounding factors, such as opportunistic experiments from ship-track or volcano eruptions (Chen et al., 2022; Toll et al., 2019), where an overall weak LWP adjustment was observed. For satellite studies, Rosenfeld et al. (2019) pointed out that cloud thickness (H) explained almost three-fourths of meteorological impacts on cloud radiative effect (CRE) and they demonstrated an overall positive LWP adjustment when separating H. However, we find that LWP adjustments become negative after constraining H in the intervals of Figure 1 (B and E), indicating the dominant effect of entrainment processes. The discrepancy may arise from their focus on samples in convective cores (top 10% of cloud optical thickness), which are closer to adiabatic, whereas our samples suggest more exchange with the free atmosphere.

Fons et al. (2023) suggested H is an important confounder using a causal approach and should be conditioned on. Here, our results indicate the physical significance of constraining H. The sensitivity of LWP adjustments to H is observed in Figure 1. In AUW region, negative LWP adjustments become weaker as H increases. Thicker clouds are less sensitive to entrainment-feedbacks with increasing N_d compared to thinner clouds (Figure 1B). In other words, LWP in different H intervals responds differently to N_d, so it is necessary to restrict H to exclude the effects of covariation. However, in ECS region, negative LWP

adjustments for clouds with H < 900 m become stronger with increasing H, while for clouds with H > 900 m, quite the contrary: it weakens with increasing H. The bidirectional sensitivity of LWP adjustments to H is likely attributed to distinct mixing characteristics among different cloud regimes in ECS region, reflecting the complex interactions between meteorological factors, clouds, and aerosols. Additionally, clouds above 800m are associated with warm invigoration (Figure 2D). In this condition, H serves as a mediator but not a confounder. This implies that constraints on H in ECS is inappropriate because they fundamentally restrict a majority of mechanisms influencing cloud vertical development.

In summary, the above results indicate that LWP adjustments depend on entrainment feedbacks with increasing N_d in AUW region. While in ECS region, LWP adjustments are results of the competition between entrainment feedbacks and warm invigoration. Given that LWP adjustment is influenced by a complex interaction of meteorological factors, we think that cloud conditions provide more reliable indications. Specifically, cloud thickness is important in AUW region, whereas aerosol loading (represented by N_d) is a better indicator in the ECS region. Therefore, the diurnal variations of these factors can provide important indications for us to investigate the potential mechanisms driving diurnal variations of LWP adjustments.

3.2 How LWP adjustments change over diurnal scale and mechanisms

In AUW region, the negative LWP adjustments strengthen from around 0800 LT to 1300 LT, reaching the strongest at –0.41, and then weakening to –0.34 (Figure 1C). In ECS region, the positive LWP adjustments exhibit two local peaks during the observation period, occurring at 1200 LT and 1600 LT, with peak values of 0.07 and 0.21, respectively (black line in Figure 1F). And two local minima LWP adjustments are observed at 0800 LT and 1400 LT, with values of –0.11 and –0.06, respectively. Meteorological conditions have a small impact on the diurnal patterns of LWP adjustments in both regions (Figure S7). Therefore, it is necessary to start with the diurnal variations of cloud properties to analyze the mechanisms behind the diurnal patterns of LWP adjustments.

AUW is one of the subtropical Sc regions over the eastern part of the ocean away from continents (Klein and Hartmann, 1993), characterized by large LTS and strong large-scale subsidence (Figure 3), which are favorable for the formation of Sc. Figure 6 depicts the diurnal variations of cloud properties in the Sc-like AUW region. The diurnal variation of LWP shows a typical pattern with a peak in the morning and a gradual reduction until early afternoon. According to previous studies, this pattern is subject to the diurnal cycle of solar insolation (Bretherton et al., 2004; Mechoso et al., 2014; Wood et al., 2002). Specifically, during the daytime, solar radiation absorption within the cloud layer and long-wave cooling at the cloud top drive the turbulent mixing within the cloud layer and inhibit turbulence to the sea surface, thus leading to the decoupling of the cloud-topped marine boundary layer (MBL) (Duynkerke and Hignett, 1993; Ghosh et al., 2005; Slingo et al., 1982). As decoupling cuts off the moisture source from the sea surface, the imbalance between entrainment drying and upward moisture flux may thin the cloud layer. The decrease of LWP before 1300 LT is primarily attributed to the lifting of the cloud base, indicating that entrainment drying originates from evaporation at the cloud base, which is in line with an early modeling study for typical Sc cloud regimes (Bougeault, 1985). After 1300 LT, the gradual reduction of solar heating hinders the intensification of decoupling and helps rebuild the turbulence between the cloud and subcloud layer. Therefore, LWP increases after 1300

LT likely due to the reconstruction of turbulence.

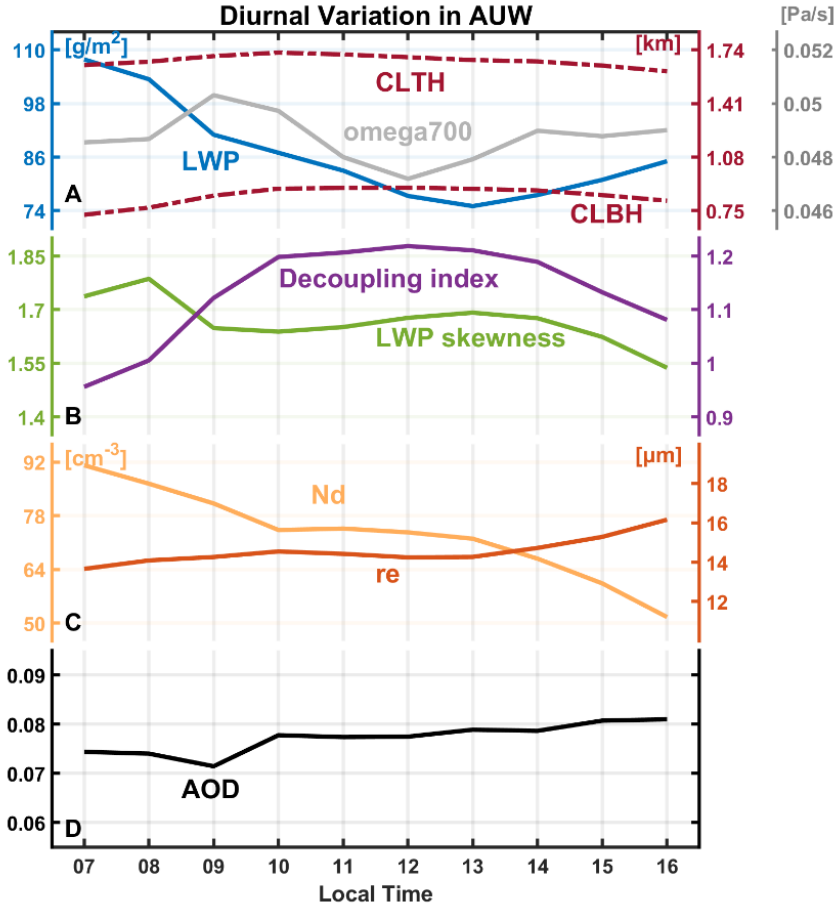

Figure 6. Diurnal patterns in AUW region. (A) Cloud liquid water path (LWP), cloud-top height (CLTH), cloud base height (CLBH) and vertical velocity on 700 hPa (omega700, positive values indicate downdraft) from ERA5 reanalysis. (B) LWP skewness and decoupling index in AUW region. (C) Cloud droplet number concentration (N_d) and effective radius (r_e). (D) Aerosol optical depth (AOD).

Following the quantification method of Zheng et al. (2018) and Kazil et al. (2017), this study presents auxiliary verifications of the decoupling process. First, according to Zheng et al. (2018), decoupling of the subtropical Sc decks during cold advection is often unstable (negative temperature advection). The formation of Cu beneath the Sc will render local coupling by feeding moisture into the upper cloud layer, thus causing a positive skewness of the probability density function (PDF) of LWP. Therefore, the skewness of LWP PDF can be used to estimate the degree of decoupling for each cloud sample:

$$\text{skewness} = \frac{\mathrm{E}(\mathrm{x}-\mathrm{u})^3}{\sigma^3} \quad (3)$$

where E is the expected value, μ and σ is the mean standard deviation of x, respectively. Positive skewness indicates more data tends to be distributed to the right, and vice versa. Larger LWP skewness indicates a larger decoupling degree.

As shown in Figure 6, LWP skewness increases before 1300 LT and then decreases, illustrating the decoupling process discussed above. Note that while the cumulus penetration alters LWP, small variations in LWP skewness suggest that it cannot be directly compared with the reduction of LWP caused by decoupling, thus having no evident effect on the diurnal variation of LWP over AUW region. Additionally, due to the fluctuation of LWP skewness before 0900 LT, another decoupling index defined by Kazil et al. (2017) is used for further indication, quantifying the relative position between the CLBH and the lifting condensation level (LCL). A larger index implies a stronger degree of decoupling:

$$\text{decoupling index} = \frac{CLBH - LCL}{LCL} \tag{4}$$

LCL is derived from ERA5 reanalysis following Wood and Bretherton (2006). The two indexes support each other and confirm the decoupling process.

Unexpectedly, there is no evident diurnal variation of AOD in AUW, but N_d continually declines from 0700 LT to 1600 LT and r_e does not change significantly before 1200 LT and then rises. It is thus reasonable to infer the diurnal variations of N_d and r_e are related with dynamic process on account of the disagreement with aerosols variations. Combing the nature of decoupling process and diurnal patterns of cloud properties in Figure 6, we discuss the possible mechanisms for the diurnal variation of N_d and r_e based on earlier cloud microphysics studies. According to Verlinden (2018), the shortwave heating counteracts longwave cooling during daytime, resulting in weakening of cloud-top entrainment. Meanwhile, the decoupling that cuts off moisture transport suppresses condensational growth. The combination of these two processes may lead to the little variation in r_e before 1200 LT. Additionally, the decoupling process leads to the suppression of both surface moisture transport and cloud base updrafts, which may in turn reduce the supersaturation and hence the number of activated cloud droplets. This may explain the continuous decrease in N_d before 1300 LT. Furthermore, according to the relationship between CLTH, w_s (always negative) and entrainment rate (w_e) ($\frac{dCLTH}{dt} = w_s + w_e$) in the mixed-layer model framework (Painemal et al., 2013), we explain the variations after 1200 LT. CLTH begins to decrease after 1200 LT, suggesting an intensification of large-scale subsidence (w_s, always negative in Sc region) and/or a weakening of entrainment rate (w_e). Large-scale subsidence on 700 hPa from ERA5 reanalysis becomes stronger (gray line in Figure 6A). It may enhance the temperature-inversion jump, which will in turn decrease the entrainment rate (Painemal et al., 2013). During this period, the condensational growth by the reconstructed water vapor supply will enhance r_e. Meanwhile, the coalescence process, enhanced by an increase in r_e leads to a decrease in N_d. This process could be more dominant than the increase in activated cloud droplets caused by water vapor reestablishment for an increase in N_d to be observed in this study.

Based on the diurnal mechanisms of MBL discussed above, the diurnal pattern of LWP adjustments is primarily a consequence of the influence of these diurnal-related mechanisms on the relationship between N_d and LWP across different microphysical-dynamical conditions. In AUW, the diurnal variations of the overall LWP adjustments (black line in Figure 1C) and cloud thickness (blue line in Figure 1C) demonstrate a strong consistency with a turning point at 1300 LT. The variation

of LWP adjustment here is mainly attributed to the gradual thinning of clouds, which reflects the differential LWP responses to N_d with varying H. LWP adjustment becomes more negative with the thinning of cloud, which is consistent with the results in Figure 1B. After 1300 LT, cloud thickness remains almost unchanged. The variation in LWP adjustments is mainly governed the weakening of entrainment due to the intensification of large-scale subsidence (Figure 6A). During this time, the weakening of the entrainment process leads to a weakening of the negative LWP adjustments over AUW region.

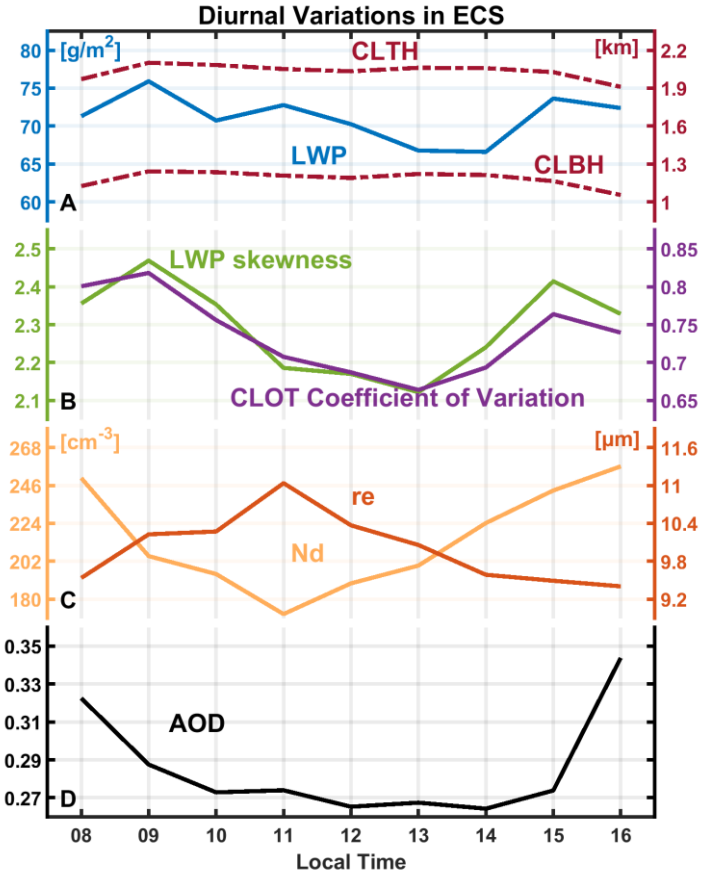

Figure 7. Diurnal patterns in ECS region. (A) Cloud liquid water path (LWP), cloud-top height (CLTH) and cloud base height (CLBH). (B) LWP skewness and coefficient of variation (c_v) of cloud optical depth (CLOT) in AUW region. (C) Cloud droplet number concentration (N_d) and effective radius (r_e). (D) Aerosol optical depth (AOD).

In contrast, conditions in MBL in ECS region are more complicated. As mentioned in the last section, ECS is a transition region due to the "deepening-warming" process. Under this condition, MBL is seldom fully coupled but exhibits local cumulus coupling. Apparently, LWP skewness is a more appropriate indicator to reflect cumulus coupling in this region. Furthermore, the spatial distribution of LWP skewness can indicate the influence of cumulus coupling offshore (Figure 4C). For diurnal variations in ECS in Figure 7, there is a general decrease in LWP before 1300 LT followed by an increase. This is in contrast

to the pronounced cloud thinning observed in the AUW region due to the decoupling of MBL by solar heating. In the ECS region, the overall change of LWP is not significant (less than 10 g/m^2). Since MBL is never fully coupled, these minor observed changes are mainly caused by local cumulus coupling. The variations of LWP and LWP skewness exhibit a strong consistency. We also calculate the coefficient of variation (c_v) of CLOT to represent the uniformity of each cloud sample. c_v is defined as the standard deviation (σ) divided by the mean(μ):

$$c_v = \frac{\sigma}{\mu} \tag{5}$$

The smaller the c_v is, the less dispersion there is among the cloud pixels in the cloud sample, resulting in a more uniform sample. It turns out that the cloud layer is influenced primarily by the strength of cumulus coupling, rather than other factors.

In the ECS region, the weakest cumulus activity occurs at 1300 LT (the lowest LWP skewness in Figure 7B), which may be attributed to solar insolation. In the Sc to Cu transition region, the decoupled cloud layer and subcloud layer are often separated by a stable transition layer, which has been widely observed by the Atlantic Stratocumulus Transition Experiment (ASTEX) conducted over the northeast Atlantic Ocean. Based on ASTEX, Rogers et al. (1995) suggested that the shortwave radiation would hinder convection during daytime by increasing the stability of the transition layer. Miller et al. (1998) extended this theory to the diurnal variations and believed that the diurnal variation of Cu development was regulated by the stability of the transition layer.

In terms of microphysical properties, N_d in ECS decreases before 1100 LT and then increases. Variations of r_e are just the opposite except insignificant change since 1400 LT. The crucial mechanism leading to such changes may be attributed to the weakest entrainment drying at 1100 LT, resulting in the highest values of r_e and lowest values of N_d. Such diurnal variations in entrainment have also been observed in other coastal areas. Caldwell et al. (2005) reported the weakest entrainment rate at 1100 LT during East Pacific Investigation of Climate (EPIC) stratocumulus cruise in 2001. Painemal et al. (2017) found the minimum of entrainment occurred between 0900-1100 LT over the northeast Pacific region, attributing the diurnal pattern to the turbulence caused by long-wave radiative cooling. Additionally, other factors may also contribute to the diurnal variations of N_d and r_e. For example, the changes before 1100 LT may include the impacts of reducing aerosol loadings. Subsidence from both cloud top and bottom occurred after 1400 LT may limit the entrainment and the continuous decline of r_e. Cumulus coupling may also contribute to the increase of N_d, Martin et al. (1995) found local increase in N_d induced by the intrusion of cumulus clouds during ASTEX.

In ECS region, based on the above mechanisms, the diurnal variation of LWP is relatively small, yet N_d exhibits a distinct diurnal pattern. Changes in N_d lead to LWP adjustments that correspond to two microphysical-dynamical processes. The turning point between the two stages exhibits the same diurnal variation as the average N_d (Figure S8). Before noon, a decrease in N_d weakens the warm invigoration (blue line in Figure 1F), while the entrainment feedback intensifies (purple line in Figure 1F). After 1200 LT, the trend reverses. The opposing patterns between warm invigoration and entrainment feedback further reflect their competitive nature. The interaction of these two processes drives the overall diurnal variation in LWP adjustments (black line in Figure 1F).

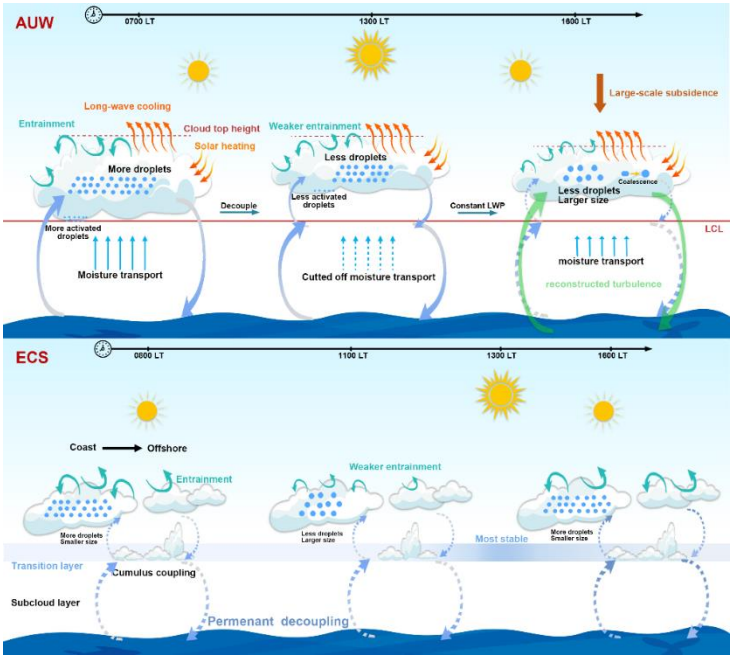

Figure 8. Schematics of diurnal dominant mechanisms observed in AUW and ECS regions. See text for details. Only the primary mechanisms are presented, while the relatively unimportant ones are omitted. Note that we represent the lifting condensation level (LCL) and transition layer at the same altitude for intuition. However, this depiction does not imply that their heights remain constant throughout the diurnal variation.

Given that the samples include four seasons over four years, we conduct a sensitivity analysis regarding seasonal influences as cloud properties and environmental conditions can vary significantly across different seasons. Overall, the diurnal pattern of LWP adjustments is not sensitive to seasonal changes in AUW region (black lines in Figures S9F-S12F compared to Figure 1). Since the AUW region is a persistent stratocumulus area, the diurnal variations of cloud thickness remain consistent across all seasons, with the thickest clouds in the morning and the thinnest in the early afternoon, followed by a slow increase. This implies that the decoupling process in the persistent Sc region is not affected by seasonality, resulting in the similar patterns of LWP adjustments. ECS region exhibits seasonal differences (Figures S9-S12). Among the total samples (173181), spring, summer, autumn, and winter account for 31%, 3%, 22%, and 44%, respectively. Due to the limited summer samples (3%), their results are statistical insignificance ($p > 0.05$), especially after eliminating the samples with precipitation by applying the threshold (GPM = 0 mm hr^{-1}). The LWP adjustments in other seasons exhibit similar diurnal patterns and magnitudes, peaking at noon (black lines in Figures S9F, S11-S12F). This similarity may be due to the weak seasonal variations in the diurnal patterns of LWP and N_d (not shown). The diurnal patterns of warm invigoration in spring and winter are similar to the overall results (blue lines in Figures S9F and S12F compared to Figure 1F). The minimum N_d at 1100 LT coincides with the weakest warm invigoration (i.e., minimal LWP enhancement). Autumn exhibits the lowest N_d among seasons (Figure

S11F), corresponding to the weakest warm invigoration (~50%/31% lower than spring/winter) and the largest diurnal fluctuations. The diurnal pattern of entrainment feedbacks in spring differs from other seasons, possibly due to its distinct entrainment rate diurnal variation, which can be illustrated by the variation of cloud-top height (CLTH). Here, based on the relationship between CLTH, w_s (always negative) and entrainment rate (w_e) ($\frac{dCLTH}{dt} = w_s + w_e$) (Painemal et al., 2013), the diurnal variations of w_e (entrainment rate) can be qualitatively analyzed with the diurnal variations of CLTH and large-scale subsidence (w_s) (Figure S13). Before 1400 LT, the variation of large-scale subsidence is unrelated to CLTH, thus the change in CLTH can only be attributed to entrainment rate. It weakens before 1200 LT, possibly due to the decreasing cloud-top longwave cooling after sunrise. It then increases until 1400 LT which may be caused by the enhanced longwave cooling. After 1400 LT, the decrease in CLTH is caused by the enhancement of large-scale subsidence.

To summarize, Figure 8 depicts schematics of the dominant mechanisms in the two regions. In AUW region the primary mechanism behind the diurnal variation of LWP adjustments is the cloud thinning driven by MBL decoupling before 1300 LT. After 1300 LT, the gradual weakening of cloud-top entrainment mitigates the negative LWP adjustments. In ECS region, the diurnal variation of LWP adjustments is jointly determined by competing microphysical-dynamical processes (i.e., entrainment feedback and warm invigoration). Failure to accurately capture these diurnal variations in LWP adjustments and the underlying physical processes in observational studies may result in substantial inaccuracies in the quantification of regional and global LWP adjustments, and the associated radiative forcing.

3.3 Impacts on aerosol indirect radiative effect if neglecting diurnal variations

Regional geostationary satellite observation reveals the significant impact of regional diurnal dynamic processes on LWP adjustments. LWP adjustments vary from –0.41 to –0.27 in AUW and from –0.11 to 0.21 in ECS. Diurnal averaged LWP adjustments are –0.31 and 0.02 considering the diurnal processes, respectively. The averaged LWP adjustment (dashed line in Figure 1, C and F) is not a simple average of the values, rather, it is derived from all available data within the region, accounting for diurnal covariation. This implies the inadequacy of previous observations only based on polar-orbiting satellites. For example, for Sc in AUW region, if LWP adjustments observed by polar-orbiting satellite (such as MODIS overpass for aqua at 1330 LT or terra at 1030 LT) are applied to represent the whole day, the negative LWP adjustments will be obviously overestimated because the polar-orbiting observations failed to capture the weaker entrainment process in the late afternoon. This bias will ultimately affect our estimation of cloud brightening in Twomey effect. The cloud albedo (A_c) susceptibility to aerosols can be estimated as (Bellouin et al. 2020):

$$S = \frac{dA_C}{dN_d} = \frac{A_C(1 - A_C)}{3N_d}\left(1 + \frac{5}{2}\frac{d\ln LWP}{d\ln N_d}\right) \quad (6)$$

where S is the sensitivity of cloud albedo. According to this equation, LWP adjustments serve to regulate the cooling effect of the Twomey effect (the first term).

Following the method of (Glassmeier et al., 2021), we assume that climatological A_c is approximated as a constant value

of the steady-state. Then the impact of LWP adjustments on S depends on $\left(1+\frac{5}{2}\frac{\mathrm{d\ln LWP}}{\mathrm{d\ln N_d}}\right)$ according to Eq. 6. If we only consider LWP adjustments at fixed moments but neglect the diurnal variations, the cooling effect of LWP adjustments (strengthen Twomey effect) will be severely underestimated. For example, the average LWP adjustments at MODIS Aqua and Terra overpasses (1030 LT and 1330 LT) are −0.39 in AUW region and -0.04 in ECS region, respectively. The daily average LWP adjustments for the two regions are −0.31 and 0.02, respectively. After substituting these values into $\left(1+\frac{5}{2}\frac{\mathrm{d\ln LWP}}{\mathrm{d\ln N_d}}\right)$, the cooling effect of LWP adjustments will be underestimated by |(0.225−0.025)/0.225|×100% = 89% in AUW region if neglecting the diurnal variations. This bias will lead to a further |(−0.39−(−0.31))/(−0.4)|×100% = 20% offset of the Twomey effect, as the Twomey effect is completely offset when the LWP adjustment is −0.4. Thereby the offset will steer aerosol indirect radiative effect towards a warming direction. Similarly, these two estimates are 14% and 15% for ECS region.

4 Discussion

Our observed diurnal LWP adjustment pattern in the AUW region is consistent with Qiu et al. (2024)'s findings in the eastern North Atlantic, where thick-thin cloud transitions dominated daytime variability. However, unlike Qiu et al. (2024)'s method, which focused on regional cloud internal evolution and calculated LWP adjustment within each 1° grid box without considering meteorological covariations, this investigation preserves the influence of meteorological covariations at each moment. By stratifying analyses by cloud thickness according to Rosenfeld et al. (2019), we disentangle meteorological covariations from cloud internal feedbacks. Additionally, cloud thickness remains relatively stable after 1300 LT in our results. The weakening of negative LWP adjustments is primarily due to the weakening of entrainment induced by the strengthening of large-scale subsidence.

Furthermore, we conduct the same analyses in ECS region with completely different environmental background, and obtain entirely different results. In humid and unstable environments, aerosol-induced warm invigoration is more likely to occur. In this condition, cloud thickness is no longer suitable for distinguishing meteorological conditions as a mediator of N_d-LWP relationship. The cloud thinning mechanism is also insufficient to explain the diurnal variations of LWP adjustments. This demonstrates that the significant regional differences in the diurnal variations of LWP adjustments, depending on aerosol loadings, cloud regimes and meteorological conditions.

It is worth noting that our results also reveal diurnal variations of N_d, a core indicator in ACI, which are also attributed to the MBL diurnal processes. While previous studies have analyzed the long-term variations of N_d, highlighting the key role of aerosols (Hu et al., 2021; Li et al., 2018; McCoy et al., 2015, 2018; Quaas et al., 2006), unexpectedly, there is no good consistency between them in diurnal variations. This discrepancy may stem from previous polar-orbiting satellite observations at fixed times have overlooked the crucial role played by other physical mechanisms at different times. Figure 5 suggests a pronounced impact of anthropogenic activities on cloud microphysical properties on a long-term scale. Note that the correlations between AOD and N_d at certain fixed times are not statistically significant (not shown). This may be due to the

relatively insignificant impact of aerosol effects at these moments, while other physical processes may exert a more pronounced influence. Future researches should broaden its scope to investigate effects of other physical processes on N_d at specific times, in addition to the roles of aerosols. Moreover, in the context of global warming, whether these physical processes will be affected and consequently contribute to variations of N_d deserves further investigation.

Several limitations should be acknowledged in this study. First, the time-dependence of LWP adjustments we discussed differs from the cloud evolution process, emphasizing diurnal variations caused by changes in dominant mechanisms at different times rather than tracking the evolution of individual clouds. This approach may introduce uncertainties into our results since the full cloud life cycle and evolution are not the same with diurnal variations. The full cloud lifetime evolution associated with LWP adjustments is not the scope of this study and warrants further exploration. Additionally, given the scarcity of observational data at fine scales, certain mechanisms are indirectly inferred from the observational index (e.g., decoupling process inferred from LWP skewness), which needs further microphysical-process-based in-situ observations as well as model simulations. Finally, uncertainties of retrievals have been discussed in Data and Methods, which provides further context for the limitations of this study.

5 Conclusion

This study reveals the diurnal variations of LWP adjustments in two specific regions within the sight of Himawari-8, along with the possible mechanisms contributing to these variations. The studied regions have significant differences in environmental conditions and aerosol loadings. Although some conclusions are similar to the previous studies, we have also discovered some new phenomena. The observational studies demonstrate LWP adjustments in two regions are determined by the dominant microphysical-dynamical processes in different N_d stages (entrainment feedbacks and warm invigoration), while their diurnal variations depend on the dynamical conditions of the boundary layer. Important findings from this investigation are as follows:

(1) In AUW region, the diurnal variations of LWP adjustments are insensitive to seasonality. The overall negative LWP adjustments decrease from −0.27 to −0.41 before 1300 LT and then increase to −0.34. Cloud thickness in AUW region can serve as a confounder to separate the effects of meteorological covariations. The diurnal pattern is primarily associated with cloud thinning induced by decoupling process of MBL quantified by LWP skewness before 1300 LT and the weakening of entrainment induced by intensification of large-scale subsidence after 1300 LT.

(2) In ECS region, diurnal variations of LWP adjustment exhibit seasonal differences. Samples from winter and spring dominate the overall variations (accounting for 75% of the total samples). For the overall results, LWP increases and then decreases with N_d, suggesting possible competition between entrainment feedbacks and warm invigoration. The diurnal pattern of LWP adjustments is determined by the combined diurnal variations of these two mechanisms. Warm invigoration is related to the diurnal variation of the N_d at the turning points of the two processes. Lower N_d in the ECS region implies a weaker warm invigoration.

(3) We indicate an overall underestimation of the cooling effect by LWP adjustment up to 89% (14%), with a further 20% (15%) offset of the Twomey effect when neglecting the diurnal variations of LWP adjustments in AUW (ECS) region. Furthermore, our results quantify the regional impact of boundary layer dynamic conditions on LWP adjustments. For example, diurnal decoupling process in AUW region results in a 219% variation of LWP adjustments within the daytime relative to the daily mean (the diurnal variation range divided by the daily mean), assuming other conditions remain relatively unchanged.

Our research provides a detailed discussion for the diurnal variations of LWP adjustments and how they are influenced by existed boundary layer mechanisms. We underscore the importance of fully considering the covariation with environmental conditions, indicating different potential influencing factors on cloud brightening and radiative forcing in terms of the regional and diurnal daytime scale. It is a highly time-dependent variable lacking quantification and should be taken into consideration of future research in aerosol indirect effects on climate.

Data availability

The datasets that support this study are all available to public. The SatCORPS Himawari-8 product is available at https://asdc.larc.nasa.gov/project/CERES. The MERRA-2 product is available at https://disc.gsfc.nasa.gov/datasets/M2T1NXAER_5.12.4/summary?keywords=merra2. The GPM_3IMERGHHV07 is available at https://disc.gsfc.nasa.gov/datasets/GPM_3IMERGHH_07/summary?keywords=gpm%20imerg. ERA5 reanalysis data is available at https://cds.climate.copernicus.eu/. All data are available in the main text or the supporting information.

Author contributions

JiaL and YaW performed the analysis and organized the original manuscript. JimL and YaW conceptualized the study and reviewed the manuscript. WZ assisted in data analysis and validation. LZ and YuW assisted in investigation and the final review and editing of the manuscript.

Competing interests

The contact author has declared that none of the authors has any competing interests.

Acknowledgments

We would like to acknowledge ChatGPT for its role in polishing the language for the text. We would like to acknowledge freepik.com for supporting icons used in our schematics (www.freepik.com).

Financial support

This work is supported by the following funding: Key Program of the National Natural Science Foundation of China (42430601), Major Program of the National Natural Science Foundation of China (42090030), National Natural Science Foundation of China (42175087), Science and Technology Project of Gansu Province (Outstanding Youth Fund, 24JRRA386).

References

Ackerman, A. S., Kirkpatrick, M. P., Stevens, D. E., and Toon, O. B.: The impact of humidity above stratiform clouds on indirect aerosol climate forcing, Nature, 432, 1014–1017, https://doi.org/10.1038/nature03174, 2004.

Albrecht, B. A.: Aerosols, Cloud Microphysics, and Fractional Cloudiness, Science, 245, 1227–1230, https://doi.org/10.1126/science.245.4923.1227, 1989.

Albrecht, B. A., Bretherton, C. S., Johnson, D., Scubert, W. H., and Frisch, A. S.: The Atlantic Stratocumulus Transition Experiment—ASTEX, Bulletin of the American Meteorological Society, 76, 889–904, https://doi.org/10.1175/1520-0477(1995)076<0889:TASTE>2.0.CO;2, 1995.

Altaratz, O., Koren, I., Remer, L. A., and Hirsch, E.: Review: Cloud invigoration by aerosols—Coupling between microphysics and dynamics, Atmospheric Research, 140–141, 38–60, https://doi.org/10.1016/j.atmosres.2014.01.009, 2014.

Bellouin, N., Quaas, J., Gryspeerdt, E., Kinne, S., Stier, P., Watson-Parris, D., Boucher, O., Carslaw, K. S., Christensen, M., Daniau, A. -L., Dufresne, J. -L., Feingold, G., Fiedler, S., Forster, P., Gettelman, A., Haywood, J. M., Lohmann, U., Malavelle, F., Mauritsen, T., McCoy, D. T., Myhre, G., Mülmenstädt, J., Neubauer, D., Possner, A., Rugenstein, M., Sato, Y., Schulz, M., Schwartz, S. E., Sourdeval, O., Storelvmo, T., Toll, V., Winker, D., and Stevens, B.: Bounding Global Aerosol Radiative Forcing of Climate Change, Rev. Geophys., 58, https://doi.org/10.1029/2019RG000660, 2020.

Bender, F. A.-M., Frey, L., McCoy, D. T., Grosvenor, D. P., and Mohrmann, J. K.: Assessment of aerosol–cloud–radiation correlations in satellite observations, climate models and reanalysis, Clim Dyn, 52, 4371–4392, https://doi.org/10.1007/s00382-018-4384-z, 2019.

Bennartz, R.: Global assessment of marine boundary layer cloud droplet number concentration from satellite, J. Geophys. Res., 112, D02201, https://doi.org/10.1029/2006JD007547, 2007.

Bennartz, R. and Rausch, J.: Global and regional estimates of warm cloud droplet number concentration based on 13 years of AQUA-MODIS observations, Atmos. Chem. Phys., 17, 9815–9836, https://doi.org/10.5194/acp-17-9815-2017, 2017.

Boers, R., Acarreta, J. R., and Gras, J. L.: Satellite monitoring of the first indirect aerosol effect: Retrieval of the droplet concentration of water clouds, Journal of Geophysical Research: Atmospheres, 111, https://doi.org/10.1029/2005JD006838, 2006.

Bougeault, P.: The Diurnal Cycle of the Marine Stratocumulus Layer: A Higher-Order Model Study, Journal of the Atmospheric Sciences, 42, 2826–2843, https://doi.org/10.1175/1520-0469(1985)042<2826:TDCOTM>2.0.CO;2, 1985.

Brenguier, J.-L., Burnet, F., and Geoffroy, O.: Cloud optical thickness and liquid water path – does the *k* coefficient vary with droplet concentration?, Atmospheric Chemistry and Physics, 11, 9771–9786, https://doi.org/10.5194/acp-11-9771-2011, 2011.

Bretherton, C. S. and Wyant, M. C.: Moisture Transport, Lower-Tropospheric Stability, and Decoupling of Cloud-Topped Boundary Layers, Journal of the Atmospheric Sciences, 54, 148–167, https://doi.org/10.1175/1520-0469(1997)054<0148:MTLTSA>2.0.CO;2, 1997.

Bretherton, C. S., Uttal, T., Fairall, C. W., Yuter, S. E., Weller, R. A., Baumgardner, D., Comstock, K., Wood, R., and Raga, G. B.: The Epic 2001 Stratocumulus Study, Bulletin of the American Meteorological Society, 85, 967–978, https://doi.org/10.1175/BAMS-85-7-967, 2004.

Bretherton, C. S., Blossey, P. N., and Uchida, J.: Cloud droplet sedimentation, entrainment efficiency, and subtropical stratocumulus albedo, Geophysical Research Letters, 34, 2006GL027648, https://doi.org/10.1029/2006GL027648, 2007.

Buchard, V., Randles, C. A., Silva, A. M. da, Darmenov, A., Colarco, P. R., Govindaraju, R., Ferrare, R., Hair, J., Beyersdorf, A. J., Ziemba, L. D., and Yu, H.: The MERRA-2 Aerosol Reanalysis, 1980 Onward. Part II: Evaluation and Case Studies, Journal of Climate, 30, 6851–6872, https://doi.org/10.1175/JCLI-D-16-0613.1, 2017.

Caldwell, P., Bretherton, C. S., and Wood, R.: Mixed-Layer Budget Analysis of the Diurnal Cycle of Entrainment in Southeast Pacific Stratocumulus, Journal of the Atmospheric Sciences, 62, 3775–3791, https://doi.org/10.1175/JAS3561.1, 2005.

Change (IPCC), I. P. on C.: The Earth's Energy Budget, Climate Feedbacks and Climate Sensitivity, in: Climate Change 2021 – The Physical Science Basis: Working Group I Contribution to the Sixth Assessment Report of the Intergovernmental Panel on Climate Change, Cambridge University Press, 923–1054, 2023.

Chen, Y., Haywood, J., Wang, Y., Malavelle, F., Jordan, G., Partridge, D., Fieldsend, J., De Leeuw, J., Schmidt, A., Cho, N., Oreopoulos, L., Platnick, S., Grosvenor, D., Field, P., and Lohmann, U.: Machine learning reveals climate forcing from aerosols is dominated by increased cloud cover, Nat. Geosci., 15, 609–614, https://doi.org/10.1038/s41561-022-00991-6, 2022.

Chen, Y.-C., Christensen, M. W., Stephens, G. L., and Seinfeld, J. H.: Satellite-based estimate of global aerosol–cloud radiative forcing by marine warm clouds, Nature Geosci, 7, 643–646, https://doi.org/10.1038/ngeo2214, 2014.

Christensen, M. W. and Stephens, G. L.: Microphysical and macrophysical responses of marine stratocumulus polluted by underlying ships: Evidence of cloud deepening, J. Geophys. Res., 116, D03201, https://doi.org/10.1029/2010JD014638, 2011.

Coakley, J. A. and Walsh, C. D.: Limits to the Aerosol Indirect Radiative Effect Derived from Observations of Ship Tracks, Journal of the Atmospheric Sciences, 59, 668–680, https://doi.org/10.1175/1520-0469(2002)059<0668:LTTAIR>2.0.CO;2, 2002.

Dagan, G., Koren, I., and Altaratz, O.: Competition between core and periphery-based processes in warm convective clouds – from invigoration to suppression, Atmospheric Chemistry and Physics, 15, 2749–2760, https://doi.org/10.5194/acp-15-2749-2015, 2015.

Duynkerke, P. G. and Hignett, P.: Simulation of Diurnal Variation in a Stratocumulus-capped Marine Boundary Layer during FIRE, Monthly Weather Review, 121, 3291–3300, https://doi.org/10.1175/1520-0493(1993)121<3291:SODVIA>2.0.CO;2, 1993.

Engström, A. and Ekman, A. M. L.: Impact of meteorological factors on the correlation between aerosol optical depth and cloud fraction: IMPACTS ON AEROSOL-CLOUD RELATIONSHIPS, Geophys. Res. Lett., 37, n/a-n/a, https://doi.org/10.1029/2010GL044361, 2010.

Feingold, G., Ghate, V. P., Russell, L. M., Blossey, P., Cantrell, W., Christensen, M. W., Diamond, M. S., Gettelman, A., Glassmeier, F., Gryspeerdt, E., Haywood, J., Hoffmann, F., Kaul, C. M., Lebsock, M., McComiskey, A. C., McCoy, D. T., Ming, Y., Mülmenstädt, J., Possner, A., Prabhakaran, P., Quinn, P. K., Schmidt, K. S., Shaw, R. A., Singer, C. E., Sorooshian, A., Toll, V., Wan, J. S., Wood, R., Yang, F., Zhang, J., and Zheng, X.: Physical science research needed to evaluate the viability and risks of marine cloud brightening, Sci. Adv., 10, eadi8594, https://doi.org/10.1126/sciadv.adi8594, 2024.

Fons, E., Runge, J., Neubauer, D., and Lohmann, U.: Stratocumulus adjustments to aerosol perturbations disentangled with a causal approach, npj Clim Atmos Sci, 6, 130, https://doi.org/10.1038/s41612-023-00452-w, 2023.

George, R. C. and Wood, R.: Subseasonal variability of low cloud radiative properties over the southeast Pacific Ocean, Atmos. Chem. Phys., 10, 4047–4063, https://doi.org/10.5194/acp-10-4047-2010, 2010.

Ghosh, S., Osborne, S., and Smith, M. H.: On the importance of cumulus penetration on the microphysical and optical properties of stratocumulus clouds, Atmospheric Chemistry and Physics, 5, 755–765, https://doi.org/10.5194/acp-5-755-2005, 2005.

Glassmeier, F., Hoffmann, F., Johnson, J. S., Yamaguchi, T., Carslaw, K. S., and Feingold, G.: Aerosol-cloud-climate cooling overestimated by ship-track data, Science, 371, 485–489, https://doi.org/10.1126/science.abd3980, 2021.

Grosvenor, D. P., Sourdeval, O., Zuidema, P., Ackerman, A., Alexandrov, M. D., Bennartz, R., Boers, R., Cairns, B., Chiu, J. C., Christensen, M., Deneke, H., Diamond, M., Feingold, G., Fridlind, A., Hünerbein, A., Knist, C., Kollias, P., Marshak, A., McCoy, D., Merk, D., Painemal, D., Rausch, J., Rosenfeld, D., Russchenberg, H., Seifert, P., Sinclair, K., Stier, P., van Diedenhoven, B., Wendisch, M., Werner, F., Wood, R., Zhang, Z., and Quaas, J.: Remote Sensing of Droplet Number Concentration in Warm Clouds: A Review of the Current State of Knowledge and Perspectives, Reviews of Geophysics, 56, 409–453, https://doi.org/10.1029/2017RG000593, 2018.

Gryspeerdt, E., Goren, T., Sourdeval, O., Quaas, J., Mülmenstädt, J., Dipu, S., Unglaub, C., Gettelman, A., and Christensen, M.: Constraining the aerosol influence on cloud liquid water path, Atmos. Chem. Phys., 19, 5331–5347, https://doi.org/10.5194/acp-19-5331-2019, 2019.

Gryspeerdt, E., Goren, T., and Smith, T. W. P.: Observing the timescales of aerosol–cloud interactions in snapshot satellite images, Atmos. Chem. Phys., 21, 6093–6109, https://doi.org/10.5194/acp-21-6093-2021, 2021.

Gryspeerdt, E., Glassmeier, F., Feingold, G., Hoffmann, F., and Murray-Watson, R. J.: Observing short-timescale cloud development to constrain aerosol–cloud interactions, Atmos. Chem. Phys., 22, 11727–11738, https://doi.org/10.5194/acp-22-11727-2022, 2022a.

Gryspeerdt, E., McCoy, D. T., Crosbie, E., Moore, R. H., Nott, G. J., Painemal, D., Small-Griswold, J., Sorooshian, A., and Ziemba, L.: The impact of sampling strategy on the cloud droplet number concentration estimated from satellite data, Atmos. Meas. Tech., 15, 3875–3892, https://doi.org/10.5194/amt-15-3875-2022, 2022b.

Hersbach, H., Bell, B., Berrisford, P., Hirahara, S., Horányi, A., Muñoz-Sabater, J., Nicolas, J., Peubey, C., Radu, R., Schepers, D., Simmons, A., Soci, C., Abdalla, S., Abellan, X., Balsamo, G., Bechtold, P., Biavati, G., Bidlot, J., Bonavita, M., De Chiara, G., Dahlgren, P., Dee, D., Diamantakis, M., Dragani, R., Flemming, J., Forbes, R., Fuentes, M., Geer, A., Haimberger, L., Healy, S., Hogan, R. J., Hólm, E., Janisková, M., Keeley, S., Laloyaux, P., Lopez, P., Lupu, C., Radnoti, G., de Rosnay, P., Rozum, I., Vamborg, F., Villaume, S., and Thépaut, J.-N.: The ERA5 global reanalysis, Quarterly Journal of the Royal Meteorological Society, 146, 1999–2049, https://doi.org/10.1002/qj.3803, 2020.

Hu, Y., Lu, X., Zhai, P.-W., Hostetler, C. A., Hair, J. W., Cairns, B., Sun, W., Stamnes, S., Omar, A., Baize, R., Videen, G., Mace, J., McCoy, D. T., McCoy, I. L., and Wood, R.: Liquid Phase Cloud Microphysical Property Estimates From CALIPSO Measurements, Front. Remote Sens., 2, https://doi.org/10.3389/frsen.2021.724615, 2021.

Huffman, G. J., Bolvin, D. T., Braithwaite, D., Hsu, K.-L., Joyce, R. J., Kidd, C., Nelkin, E. J., Sorooshian, S., Stocker, E. F., Tan, J., Wolff, D. B., and Xie, P.: Integrated Multi-satellite Retrievals for the Global Precipitation Measurement (GPM) Mission (IMERG), in: Satellite Precipitation Measurement: Volume 1, edited by: Levizzani, V., Kidd, C., Kirschbaum, D. B., Kummerow, C. D., Nakamura, K., and Turk, F. J., Springer International Publishing, Cham, 343–353, https://doi.org/10.1007/978-3-030-24568-9_19, 2020.

Jian, B., Li, J., Wang, G., Zhao, Y., Li, Y., Wang, J., Zhang, M., and Huang, J.: Evaluation of the CMIP6 marine subtropical stratocumulus cloud albedo and its controlling factors, Atmos. Chem. Phys., 21, 9809–9828, https://doi.org/10.5194/acp-21-9809-2021, 2021.

Jiang, X., Su, H., Jiang, J. H., Neelin, J. D., Wu, L., Tsushima, Y., and Elsaesser, G.: Muted extratropical low cloud seasonal cycle is closely linked to underestimated climate sensitivity in models, Nat Commun, 14, 5586, https://doi.org/10.1038/s41467-023-41360-0, 2023.

Kang, L., Marchand, R., and Smith, W.: Evaluation of MODIS and Himawari-8 Low Clouds Retrievals Over the Southern Ocean With In Situ Measurements From the SOCRATES Campaign, Earth and Space Science, 8, https://doi.org/10.1029/2020EA001397, 2021.

Kaufman, Y. J., Koren, I., Remer, L. A., Rosenfeld, D., and Rudich, Y.: The effect of smoke, dust, and pollution aerosol on shallow cloud development over the Atlantic Ocean, Proc. Natl. Acad. Sci. U.S.A., 102, 11207–11212, https://doi.org/10.1073/pnas.0505191102, 2005.

Kazil, J., Yamaguchi, T., and Feingold, G.: Mesoscale organization, entrainment, and the properties of a closed-cell stratocumulus cloud, Journal of Advances in Modeling Earth Systems, 9, 2214–2229, https://doi.org/10.1002/2017MS001072, 2017.

Klein, S. A. and Hartmann, D. L.: The Seasonal Cycle of Low Stratiform Clouds, Journal of Climate, 6, 1587–1606, https://doi.org/10.1175/1520-0442(1993)006<1587:TSCOLS>2.0.CO;2, 1993.

Koren, I., Dagan, G., and Altaratz, O.: From aerosol-limited to invigoration of warm convective clouds, Science, 344, 1143–1146, https://doi.org/10.1126/science.1252595, 2014.

Li, J., Jian, B., Huang, J., Hu, Y., Zhao, C., Kawamoto, K., Liao, S., and Wu, M.: Long-term variation of cloud droplet number concentrations from space-based Lidar, Remote Sensing of Environment, 213, 144–161, https://doi.org/10.1016/j.rse.2018.05.011, 2018.

Manshausen, P., Watson-Parris, D., Christensen, M. W., Jalkanen, J.-P., and Stier, P.: Invisible ship tracks show large cloud sensitivity to aerosol, Nature, 610, 101–106, https://doi.org/10.1038/s41586-022-05122-0, 2022.

Martin, G. M., Johnson, D. W., and Spice, A.: The Measurement and Parameterization of Effective Radius of Droplets in Warm Stratocumulus Clouds, Journal of the Atmospheric Sciences, 51, 1823–1842, https://doi.org/10.1175/1520-0469(1994)051<1823:TMAPOE>2.0.CO;2, 1994.

Martin, G. M., Johnson, D. W., Rogers, D. P., Jonas, P. R., Minnis, P., and Hegg, D. A.: Observations of the Interaction between Cumulus Clouds and Warm Stratocumulus Clouds in the Marine Boundary Layer during ASTEX, Journal of the Atmospheric Sciences, 52, 2902–2922, https://doi.org/10.1175/1520-0469(1995)052<2902:OOTIBC>2.0.CO;2, 1995.

McCoy, D. T., Burrows, S. M., Wood, R., Grosvenor, D. P., Elliott, S. M., Ma, P.-L., Rasch, P. J., and Hartmann, D. L.: Natural aerosols explain seasonal and spatial patterns of Southern Ocean cloud albedo, Sci. Adv., 1, e1500157, https://doi.org/10.1126/sciadv.1500157, 2015.

McCoy, D. T., Bender, F. A.-M., Grosvenor, D. P., Mohrmann, J. K., Hartmann, D. L., Wood, R., and Field, P. R.: Predicting decadal trends in cloud droplet number concentration using reanalysis and satellite data, Atmos. Chem. Phys., 18, 2035–2047, https://doi.org/10.5194/acp-18-2035-2018, 2018.

Mechoso, C. R., Wood, R., Weller, R., Bretherton, C. S., Clarke, A. D., Coe, H., Fairall, C., Farrar, J. T., Feingold, G., Garreaud, R., Grados, C., McWilliams, J., Szoeke, S. P. de, Yuter, S. E., and Zuidema, P.: Ocean–Cloud–Atmosphere–Land Interactions in the Southeastern Pacific: The VOCALS Program, Bulletin of the American Meteorological Society, 95, 357–375, https://doi.org/10.1175/BAMS-D-11-00246.1, 2014.

Michibata, T., Suzuki, K., Sato, Y., and Takemura, T.: The source of discrepancies in aerosol–cloud–precipitation interactions between GCM and A-Train retrievals, Atmos. Chem. Phys., 16, 15413–15424, https://doi.org/10.5194/acp-16-15413-2016, 2016.

Miller, M. A., Jensen, M. P., and Clothiaux, E. E.: Diurnal Cloud and Thermodynamic Variations in the Stratocumulus Transition Regime: A Case Study Using In Situ and Remote Sensors, Journal of the Atmospheric Sciences, 55, 2294–2310, https://doi.org/10.1175/1520-0469(1998)055<2294:DCATVI>2.0.CO;2, 1998.

Miller, S. D., Rogers, M. A., Haynes, J. M., Sengupta, M., and Heidinger, A. K.: Short-term solar irradiance forecasting via satellite/model coupling, Solar Energy, 168, 102–117, https://doi.org/10.1016/j.solener.2017.11.049, 2018.

Min, Q., Joseph, E., Lin, Y., Min, L., Yin, B., Daum, P. H., Kleinman, L. I., Wang, J., and Lee, Y.-N.: Comparison of MODIS cloud microphysical properties with in-situ measurements over the Southeast Pacific, Atmospheric Chemistry and Physics, 12, 11261–11273, https://doi.org/10.5194/acp-12-11261-2012, 2012.

Minnis, P., Sun-Mack, S., Young, D. F., Heck, P. W., Garber, D. P., Chen, Y., Spangenberg, D. A., Arduini, R. F., Trepte, Q. Z., Smith, W. L., Ayers, J. K., Gibson, S. C., Miller, W. F., Hong, G., Chakrapani, V., Takano, Y., Liou, K.-N., Xie, Y., and

Yang, P.: CERES Edition-2 Cloud Property Retrievals Using TRMM VIRS and Terra and Aqua MODIS Data—Part I: Algorithms, IEEE Trans. Geosci. Remote Sensing, 49, 4374–4400, https://doi.org/10.1109/TGRS.2011.2144601, 2011.

Minnis, P., Sun-Mack, S., Chen, Y., Chang, F.-L., Yost, C. R., Smith, W. L., Heck, P. W., Arduini, R. F., Bedka, S. T., Yi, Y., Hong, G., Jin, Z., Painemal, D., Palikonda, R., Scarino, B. R., Spangenberg, D. A., Smith, R. A., Trepte, Q. Z., Yang, P., and Xie, Y.: CERES MODIS Cloud Product Retrievals for Edition 4—Part I: Algorithm Changes, IEEE Transactions on Geoscience and Remote Sensing, 59, 2744–2780, https://doi.org/10.1109/TGRS.2020.3008866, 2021.

NASA/LARC/SD/ASDC: SatCORPS CERES GEO Edition 4 Himawari-8 Northern Hemisphere Version 1.2, 2018a.

NASA/LARC/SD/ASDC: SatCORPS CERES GEO Edition 4 Himawari-8 Southern Hemisphere Version 1.2, 2018b.

Painemal, D. and Zuidema, P.: Assessment of MODIS cloud effective radius and optical thickness retrievals over the Southeast Pacific with VOCALS-REx in situ measurements, Journal of Geophysical Research: Atmospheres, 116, https://doi.org/10.1029/2011JD016155, 2011.

Painemal, D., Minnis, P., and O'Neill, L.: The Diurnal Cycle of Cloud-Top Height and Cloud Cover over the Southeastern Pacific as Observed by GOES-10, Journal of the Atmospheric Sciences, 70, 2393–2408, https://doi.org/10.1175/JAS-D-12-0325.1, 2013.

Painemal, D., Xu, K., Palikonda, R., and Minnis, P.: Entrainment rate diurnal cycle in marine stratiform clouds estimated from geostationary satellite retrievals and a meteorological forecast model, Geophysical Research Letters, 44, 7482–7489, https://doi.org/10.1002/2017GL074481, 2017.

Qiu, S., Zheng, X., Painemal, D., Terai, C., and Zhou, X.: Diurnal variation of aerosol indirect effect for warm marine boundary layer clouds in the eastern north Atlantic, Clouds and Precipitation/Remote Sensing/Troposphere/Physics (physical properties and processes), https://doi.org/10.5194/egusphere-2023-1676, 2023.

Qiu, S., Zheng, X., Painemal, D., Terai, C. R., and Zhou, X.: Daytime variation in the aerosol indirect effect for warm marine boundary layer clouds in the eastern North Atlantic, Atmospheric Chemistry and Physics, 24, 2913–2935, https://doi.org/10.5194/acp-24-2913-2024, 2024.

Qu, X., Hall, A., Klein, S. A., and DeAngelis, A. M.: Positive tropical marine low-cloud cover feedback inferred from cloud-controlling factors, Geophys. Res. Lett., 42, 7767–7775, https://doi.org/10.1002/2015GL065627, 2015.

Quaas, J., Boucher, O., and Lohmann, U.: Constraining the total aerosol indirect effect in the LMDZ and ECHAM4 GCMs using MODIS satellite data, Atmospheric Chemistry and Physics, 6, 947–955, https://doi.org/10.5194/acp-6-947-2006, 2006.

Rahu, J., Trofimov, H., Post, P., and Toll, V.: Diurnal Evolution of Cloud Water Responses to Aerosols, JGR Atmospheres, 127, https://doi.org/10.1029/2021JD035091, 2022.

Rogers, D. P., Yang, X., Norris, P. M., Johnson, D. W., Martin, G. M., Friehe, C. A., and Berger, B. W.: Diurnal Evolution of the Cloud-Topped Marine Boundary Layer. Part I: Nocturnal Stratocumulus Development, Journal of the Atmospheric Sciences, 52, 2953–2966, https://doi.org/10.1175/1520-0469(1995)052<2953:DEOTCT>2.0.CO;2, 1995.

Rosenfeld, D., Zhu, Y., Wang, M., Zheng, Y., Goren, T., and Yu, S.: Aerosol-driven droplet concentrations dominate coverage and water of oceanic low-level clouds, Science, 363, eaav0566, https://doi.org/10.1126/science.aav0566, 2019.

Rosenfeld, D., Kokhanovsky, A., Goren, T., Gryspeerdt, E., Hasekamp, O., Jia, H., Lopatin, A., Quaas, J., Pan, Z., and Sourdeval, O.: Frontiers in Satellite-Based Estimates of Cloud-Mediated Aerosol Forcing, Reviews of Geophysics, 61, e2022RG000799, https://doi.org/10.1029/2022RG000799, 2023.

Slingo, A., Nicholls, S., and Schmetz, J.: Aircraft observations of marine stratocumulus during JASIN, Quart J Royal Meteoro Soc, 108, 833–856, https://doi.org/10.1002/qj.49710845807, 1982.

Small, J. D., Chuang, P. Y., Feingold, G., and Jiang, H.: Can aerosol decrease cloud lifetime?, Geophys. Res. Lett., 36, L16806, https://doi.org/10.1029/2009GL038888, 2009.

Smalley, K. M., Lebsock, M. D., and Eastman, R.: Diurnal Patterns in the Observed Cloud Liquid Water Path Response to Droplet Number Perturbations, Geophysical Research Letters, 51, e2023GL107323, https://doi.org/10.1029/2023GL107323, 2024.

Toll, V., Christensen, M., Quaas, J., and Bellouin, N.: Weak average liquid-cloud-water response to anthropogenic aerosols, Nature, 572, 51–55, https://doi.org/10.1038/s41586-019-1423-9, 2019.

Trepte, Q. Z., Minnis, P., Sun-Mack, S., Yost, C. R., Chen, Y., Jin, Z., Hong, G., Chang, F.-L., Smith, W. L., Bedka, K. M., and Chee, T. L.: Global Cloud Detection for CERES Edition 4 Using Terra and Aqua MODIS Data, IEEE Transactions on Geoscience and Remote Sensing, 57, 9410–9449, https://doi.org/10.1109/TGRS.2019.2926620, 2019.

Trofimov, H., Bellouin, N., and Toll, V.: Large-Scale Industrial Cloud Perturbations Confirm Bidirectional Cloud Water Responses to Anthropogenic Aerosols, JGR Atmospheres, 125, https://doi.org/10.1029/2020JD032575, 2020.

Twomey, S.: The Influence of Pollution on the Shortwave Albedo of Clouds, Journal of the Atmospheric Sciences, 34, 1149–1152, https://doi.org/10.1175/1520-0469(1977)034<1149:TIOPOT>2.0.CO;2, 1977.

Marine Low Clouds : Radiation, Turbulence, and Forecasting:

Wilcox, E. M.: Stratocumulus cloud thickening beneath layers of absorbing smoke aerosol, Atmospheric Chemistry and Physics, 10, 11769–11777, https://doi.org/10.5194/acp-10-11769-2010, 2010.

Wood, R. and Bretherton, C. S.: On the Relationship between Stratiform Low Cloud Cover and Lower-Tropospheric Stability, Journal of Climate, 19, 6425–6432, https://doi.org/10.1175/JCLI3988.1, 2006.

Wood, R. and Hartmann, D. L.: Spatial Variability of Liquid Water Path in Marine Low Cloud: The Importance of Mesoscale Cellular Convection, Journal of Climate, 19, 1748–1764, https://doi.org/10.1175/JCLI3702.1, 2006.

Wood, R., Bretherton, C. S., and Hartmann, D. L.: Diurnal cycle of liquid water path over the subtropical and tropical oceans: DIURNAL CYCLE OF LIQUID WATER PATH, Geophys. Res. Lett., 29, 7-1-7–4, https://doi.org/10.1029/2002GL015371, 2002.

Yuan, T., Remer, L. A., and Yu, H.: Microphysical, macrophysical and radiative signatures of volcanic aerosols in trade wind cumulus observed by the A-Train, Atmospheric Chemistry and Physics, 11, 7119–7132, https://doi.org/10.5194/acp-11-7119-2011, 2011.

Zhang, J. and Feingold, G.: Distinct regional meteorological influences on low-cloud albedo susceptibility over global marine stratocumulus regions, Atmospheric Chemistry and Physics, 23, 1073–1090, https://doi.org/10.5194/acp-23-1073-2023, 2023.

Zhang, X., Wang, H., Che, H.-Z., Tan, S.-C., Yao, X.-P., Peng, Y., and Shi, G.-Y.: Radiative forcing of the aerosol-cloud interaction in seriously polluted East China and East China Sea, Atmospheric Research, 252, 105405, https://doi.org/10.1016/j.atmosres.2020.105405, 2021.

Zheng, Y., Rosenfeld, D., and Li, Z.: Estimating the Decoupling Degree of Subtropical Marine Stratocumulus Decks From Satellite, Geophysical Research Letters, 45, 12,560-12,568, https://doi.org/10.1029/2018GL078382, 2018.